Atmos. Meas. Tech. Discuss., 7, 7753–7792, 2014
www.atmos-meas-tech-discuss.net/7/7753/2014/
doi:10.5194/amtd-7-7753-2014

Atmospheric Measurement Techniques Discussions
Open Access

Retrieval of daytime total columnar water vapour from MODIS measurements over land surfaces

H. Diedrich, R. Preusker, R. Lindstrot, and J. Fischer

Institut für Weltraumwissenschaften, Freie Universität Berlin, Carl-Heinrich-Becker-Weg 6–10, 12165 Berlin, Germany

Received: 21 May 2014 – Accepted: 16 July 2014 – Published: 29 July 2014

Correspondence to: H. Diedrich (hannesd@wew.fu-berlin.de)

Published by Copernicus Publications on behalf of the European Geosciences Union.

Abstract

A retrieval of total column water vapour (TCWV) from MODIS (Moderate-resolution Imaging Spectroradiometer) measurements is presented. The algorithm is adapted from a retrieval for MERIS (Medium Resolution Imaging Spectrometer) from Lindstrot et al. (2012). It obtains the TCWV for cloud-free scenes above land at spatial resolution of 1 km × 1 km and provides uncertainties on a pixel-by-pixel basis. The algorithm has been extended by introducing correction coefficients for the transmittance calculation within the forward operator. With that a wet bias of the MODIS algorithm against ARM-Microwave Radiometer data has been eliminated. An extensive validation against other ground-based measurements (GNSS-water vapour stations, GUAN Radiosondes) on a global scale reveals a bias between −0.8 and −1.6 mm and root mean square deviations between 0.9 and 1.9 mm. This is an improvement in comparison to the operational TCWV Level 2 product (bias between −1.9 and −3.2 mm and root mean square deviations between 1.9 and 2.7 mm).

1 Introduction

1.1 Background

The bulk of water contained in the earth's atmosphere exists in the form of water vapour. It is the primary Greenhouse gas of the Earth-atmosphere system and plays an important role for the exchange of energy through the vertical and horizontal transport of latent heat. Moreover, the geographical distribution and movement of water vapour determines the distribution of clouds and occurrence of precipitation on Earth. While on short time scales, water vapour is important for, e.g. driving weather systems, on long time scales, the amount of water vapour in the atmosphere is highly relevant for the evolution of the global climate. As a consequence, the Glocal Climate Observing System (GCOS) declared the total column of water vapour (TCWV) as an

AMTD
7, 7753–7792, 2014

Essential Climate Variable (ECV), with the defined goal, to provide long time series of TCWV in sufficiently high resolution to enable the determination of both local and global trends (GCOS, 2010). Although in low spatial resolution, water vapour remote sensing over the oceans is done since the 1980s with microwave radiometers (e.g. with SSM/I: Schluessel and Emery, 1990). Trenberth et al. (2005) found a positive trend of 0.41 mm per decade for the TCWV over the ocean between 1988 and 2003.

Detecting TCWV over land is a rather challenging task because of the high heterogeneity of the (unknown) surface properties. However, there are some existing TCWV retrieval schemes using radiation measurements in the visible (VIS) (e.g. with GOME: Noël et al., 2002) or in the infrared (IR) (e.g. with IASI, Pougatchev et al., 2009) or in the near infrared (NIR) (e.g. for MERIS: Lindstrot et al., 2012). The region between 0.9 and 1 µm, called the $\rho\sigma\tau$-band, is very suitable for water vapour remote sensing, due to the fact that all surface types are sufficiently bright in this spectral interval. Lindstrot et al. (2012) introduced a procedure to retrieve TCWV for cloud-free scenes for MERIS (Medium Resolution Imaging Spectrometer) measurements with extensive error estimates on a pixel-by-pixel basis. It is based on the evaluation of the differential absorption using a band in the absorption region and one close by without any absorption features. In order to provide a dataset with global coverage and high quality over both land and ocean, a combined dataset of MERIS and SSM/I retrievals was generated in the framework of the ESA Data User Element GlobVapour project (Lindstrot et al., 2014). Unfortunately, contact to ENVISAT (ENVironmental Satellite) was lost in April 2012 and the TCWV time series has been interrupted.

Ocean and Land Color Instrument (OLCI), the follower of MERIS, is not going to be in space before 2015. An alternative, gap-filling TCWV-data-set could be the MOD05-Level2-data-set from NASA (National Aeronautics and Space Administration). It uses measurements in the NIR from MODIS (MODerate Resolution Imaging Spectroradiometer) to retrieve TCWV (Gao and Kaufman, 2003). This operational product has been provided since 1999. Unfortunately, the accuracy of this product is limited and it has not been improved since then. Here, we validated the data with global

AMTD
7, 7753–7792, 2014

ground-based measurements for the first time. Figure 1 shows the comparison of MOD05-TCWV values to MWR (MicroWave Radiometer) and GNSS (Global Navigation Satellite System) stations (see Sect. 3.4 for detailed description of the validation-data-sets). It reveals that the algorithm overestimates the TCWV by around 20 %, which is very unsatisfactory considering the desire of determining small trends in the TCWV field.

As a consequence, we adapted the procedure of Lindstrot et al. (2012) to the MODIS band-setup (see Sect. 1.2) in order to produce a precise TCWV data-set that can fill the gap between MERIS and OLCI. The new retrieval has some improvements and advantages in comparison to the operational L2-algorithm from Gao and Kaufman (2003):

1. The temperature- and humidity profile is not fixed. The atmospheric transmittance for each pixel is calculated from a mixed profile. This reduces the uncertainty of the forward operator significantly.

2. The procedure regards scattering processes on aerosols and its interaction with water vapour.

3. The TCWV is derived with the help of an inverse modeling scheme. Deviations between modeled and measured radiances in the three absorption bands are iteratively optimized with the Newton method by changing the water vapour amount. The sensitivity of each band is calculated for each retrieval step, not by fixed weighting functions.

4. Uncertainty estimates considering all error influences are given on a pixel by pixel basis.

1.2 The Moderate Resolution Imaging Spectroradiometer (MODIS)

MODIS is a 36-band scanning radiometer covering the spectral range between 0.4 and 14.4 µm and with a spatial resolution between 250 to 1 km depending on the band. It is mounted on both polar orbiting EOS (Earth Observing System) platforms Terra

AMTD
7, 7753–7792, 2014

(10.30 a.m. equator crossing time, descending) and Aqua (1.30 p.m. equator crossing time, ascending). A two sided paddle-wheel mirror scans in a field of view of 110 degrees and with the swath of 2330 km. Thus, global coverage can be provided between one and two days. MODIS bands are located on four separate focal plane assembles (FPAs) depending to their spectral positions and aligned in cross-track direction. Detectors of each spectral band are aligned in the along-track direction. Ten detectors, each with slight differences of their relative spectral response, scan the earth simultaneously with a nadir spatial resolution of 1 km × 1 km per pixel in the NIR. Five bands in the NIR region between 0.8 and 1.3 µm are used for the TCWV retrieval (see Table 1 and Fig. 3). The bands 2 and 5 (865 and 1240 nm) are located in regions with hardly any water vapour absorption features and are usually used for the remote sensing of vegetation and clouds. In the TCWV retrieval, these bands are used to estimate the surface reflectance in the $\rho\sigma\tau$-band. Bands 17, 18, 19 (905, 936, 940 nm) are water vapour absorption bands, with different strength of absorption. In band 18 absorption is more pronounced and is therefore still sensible to small TCWV values, while the weak absorption band 17 is sensitive to high TCVW values without being saturated.

2 Physical background of the retrieval method

Water vapour has various absorption features in the solar and terrestrial spectrum which is due to a combination of the three fundamental vibration modes of the water molecule. Measurements of reflected sunlight in this absorption bands enables a determination of TCWV provided that the following conditions are given:

1. Solar radiation is available, limiting the retrieval to daytime measurements.
2. The band used is located in a sufficient sensitive part of the spectrum, and is not saturated.
3. The surface albedo is sufficiently bright and can be accurately estimated, precluding dark ocean surfaces.

AMTD
7, 7753–7792, 2014

4. The photon paths through the atmosphere and the reflection function of the surface are known.

5. The lower troposphere, holding the main part of the TCWV, is not masked by clouds or optical thick aerosol layers.

The NIR MODIS bands (see Table 1 and Fig. 3) are perfectly suited for daytime, cloud-free retrieval of TCWV over land. At this spectral range, almost all surfaces provide a good background. The retrieval is based on the differential absorption technique (Gao et al. (1993); Bartsch et al. (1996); Albert et al., 2001, 2005). The basic principle of the method is the comparison of the measured radiance in an absorption band to a close-by band with no or few absorption features.

Following Hansen and Travis (1974) and Fraser et al. (1992) the radiance on the top-of-atmosphere (TOA), $L_{\mathrm{TOA}}(\lambda)$, at a certain wavelength or band can be approximated as (simplified form) :

$$L_{\mathrm{TOA}}(\lambda) = E_0(\lambda) \cdot \alpha(\lambda) \cdot T_{\mathrm{noscat}}(\lambda) \cdot \cos(\theta_{\mathrm{s}})/\pi + L_{\mathrm{path}}(\lambda) \quad (1)$$

where λ is the wavelength, $E_0(\lambda)$ the top-of-atmosphere solar flux (solar constant at the wavelength), $T_{\mathrm{noscat}}(\lambda)$ the total atmospheric transmittance without scattering, $\alpha(\lambda)$ the surface reflectance, θ_{s} the solar zenith angle and $L_{\mathrm{path}}(\lambda)$ is the radiance from scattering along the light path.

For monochromatic radiation, neglecting scattering processes along the photon path, the transmittance T through the atmosphere can be related to its optical depth τ and the air mass μ, following the Beer–Lambert law:

$$T = \exp(-\tau/\mu). \quad (2)$$

The optical depth of medium is a measure of mass of absorbing and scattering species on the photon path in the considered band. The depth and width of the individual water vapour absorption lines result from pressure- and temperature dependent broadening

AMTD
7, 7753–7792, 2014

processes. Consequently, the knowledge of the actual temperature profile and the surface pressure is necessary in order to simulate the correct atmospheric transmittance. Lindstrot et al. (2012) stated, that the error of a TCWV retrieval can be significantly reduced if:

1. The surface pressure reduction due to the surface elevation is accounted for, instead of taking a standard value.

2. The actual surface temperature is used to approximate the transmittance corresponding to the actual temperature profile by adequately mixing the pre-calculated transmittance values corresponding to the two closest standard profiles (Lindstrot and Preusker, 2012)

In Eq. (1), $L_{\text{path}}(\lambda)$ accounts for the shortening of the photon path because of scattering at aerosols and is usually only a few percent of the direct reflected solar radiation in the NIR region. In the retrieval of TCWV a scattering factor f accounts for this effect. It is defined as:

$$f = T/T_{\text{noscat}}. \tag{3}$$

where T is the true atmospheric transmittance including scattering and T_{noscat} the atmospheric transmittance in case of pure absorption. f is usually larger than one, as atmospheric scattering causes a shortening of the average photon path length and reduces the amount of TCWV, by preventing a fraction of photons from traversing the humid lower troposphere. Additionally, f is increased above dark surfaces, as the majority of the photons are reflected by atmospheric scatterers and thus do not travel through the whole vertical column of water vapour. One important parameter determining f is thus the surface reflectance (see Lindstrot et al., 2012, for detailed discussion concerning f) .

AMTD
7, 7753–7792, 2014

3 1-D-Var retrieval algorithm

The algorithm uses the information from three absorption and two framing window bands. This leads to some changes in procedure in comparison to Lindstrot et al. (2012):

- TOA-radiances are simulated for each absorption band and then compared to the measurements instead of a transmittance ratio (see Sec. 3.1)
- As an inversion technique the Newton method is used not the secant method (see Sect 3.2).
- The surface reflectance in each band is now determined from an interpolation between the positions of the window bands instead of an extrapolation from the 800–900 nm region.
- The aerosol optical depth is extracted from MODIS-L2 Data.

Additionally, we regarded more error influences in the uncertainty estimation (see Sect. 3.3)

3.1 Forward model

The forward model simulates the TOA-radiances in the absorption bands. The introduction of the scattering factor f simplifies Eq. (1):

$$L_{\mathrm{TOA}}(\lambda) = E_0(\lambda) \cdot \alpha(\lambda) \cdot T_{\mathrm{noscat}}(\lambda) \cdot f \cdot \cos(\theta_{\mathrm{s}})/\pi \tag{4}$$

As θ_{s} and $E_0(\lambda)$ are known, the following values have to be derived in the forward operator: The surface reflectance, the atmospheric transmittance and the scattering correction factor at the corresponding wavelength.

The pure absorption part of the simulated transmittance T_{noscat} is derived from pre-calculated absorption coefficients stored in look-up tables on 27 different pressure

AMTD
7, 7753–7792, 2014

levels for 6 standard profiles (McClatchey et al., 1972). The transmittance is calculated for the four look-up table grid points closest to the actual surface pressure and temperature of the considered scene, thereby assuming that the surface temperature is highly correlated with the actual vertical temperature profile. The actual surface temperature is taken from NWP reanalysis data (ERA interim 2 m-Temperature; http://data-portal.ecmwf.int/data/d/interim_daily/). The actual surface pressure is derived from converting land elevation to pressure, using the GTOPO30 digital elevation model (US GeologicalSurvey, 1996). In order to optain the surface reflectance in the corresponding absorption band, first, the two window bands are corrected for the influence of scattering as well as the small but significant influence of water vapour absorption (see Fig. 3) with a look-up table approach. This atmospheric correction requires knowledge about the aerosol loading, type and vertical distribution. However, over bright land surfaces the influence of aerosols on the retrieved surface reflectance is weak. The aerosol optical depth (AOD) is extracted from MODIS-L2 aerosol data (MOD04). For missing values a climatological standard value is taken ($AOD_{550} = 0.1$).

Afterwards, surface reflectance of the absorption band is linearly interpolated from the window bands. This requires the assumption that the surface reflectance changes linearly with wavelength in this spectral range, which is true in most cases as shown in (Gao and Kaufman, 2003). This is certainly a source of error but is accounted for in the uncertainty estimation. The correction for the water vapour absorption in the window bands is done by applying the first guess (see Sect. 3.2).

The scattering correction factor f has been calculated beforehand from radiative transfer simulations and stored in look-up tables. For this reason the Matrix Operator MOdel (MOMO, Fischer and Grassl (1984), Fell and Fischer (2001), Hollstein and Fischer, 2012) was used to derive TOA radiances for different TCWV-, AOD-, Lambertian surface reflectance values, sun zenith angles (SZA), viewing zenith angles (VZA), and relative azimuth angles (RAA).

AMTD
7, 7753–7792, 2014

3.2 Inversion technique

Only one state vector variable has to be found in the iterative optimization routine: The total column water vapour. Starting with the first guess, TCWV is adapted by minimizing the differences between simulated and measured radiances. The TCWV value for the next iteration step is derived by the following scheme after Rodgers (2000):

$$\mathbf{G} = (\mathbf{K}^T \mathbf{S_e}^{-1} \mathbf{K})^{-1} (\mathbf{K}^T \mathbf{S_e}^{-1})$$
$$x_{i+1} = x_i + (\mathbf{G}(\boldsymbol{y} - \boldsymbol{F}_i))$$

where $\mathbf{K}$ is the Jacobian matrix that contains the partial derivatives of the radiance to the TCWV value in each band, $\mathbf{S_e}$ the measurement error covariance matrix which contains the measured radiance scaled with the signal to noise ratio (SNR) for each band. $\boldsymbol{y}$ contains the measured and $\boldsymbol{F}_i$ the modeled radiances. The first guess of TCWV is obtained from a simple regression, relating TCWV to a third order polynomial of $\ln(T_{\text{noscat}})$ for band 17. The regression coefficients (c_i) were determined using the absorption forward operator (see Table 2).

3.3 Uncertainty estimate

After the iteration procedure the retrieval uncertainty is calculated, taking into account the following sources of uncertainty:

- residual model error
- instrument uncertainty (SNR)
- uncertainty of the aerosol optical depth
- uncertainty due to the missing information of the aerosol type and scale height.
- uncertainty of the surface pressure and -temperature

AMTD
7, 7753–7792, 2014

– uncertainty due to the missing information about the true temperature profile

– uncertainty due to the estimation of the surface reflectance and its spectral slope

For the error quantification, these model parameter uncertainties assembled in the error covariance matrix $\mathbf{S}_b$ are propagated into the measurement space using the standard error propagation and added to the measurement error covariance matrix $\mathbf{S_e}$:

$$\mathbf{S_y} = \mathbf{S_e} + \mathbf{K}_b^T \mathbf{S}_b \mathbf{K}_b \tag{5}$$

where $\mathbf{K}_b$ is the parameter Jacobian. The resulting error covariance matrix $\mathbf{S_y}$ is then propagated into the state vector space using the Jacobian $\mathbf{K}$. The resulting error covariance matrix $\hat{\mathbf{S}}$ is a direct measure of uncertainty in TCWV space (Rodgers, 2000):

$$\hat{\mathbf{S}} = (\mathbf{K}^T \mathbf{S_y}^{-1} \mathbf{K})^{-1}. \tag{6}$$

In the following, it is described, how the individual error sources are estimated. As outlined in Sect. 2, the scattering factor f is affected most by the surface reflectance, aerosol height and -optical thickness. For each of these parameters a perturbed f^* is calculated from the look-up tables, by perturbing the input accordingly. There is no information available about the aerosol scale height and the type (size distribution, absorption and scattering properties). Consequently, a f^* was calculated presuming an aerosol layer in the upper troposphere. Additionally, a f^* was calculated from simulations supposing another aerosol model. These f^* were used to derive perturbed TOA-radiances L^*_{TOA}. Finally, the difference $(\Delta L)^2 = (L_{\mathrm{TOA}} - L^*_{\mathrm{TOA}})^2$ is added to the measurement error variance $\mathbf{S_e}$.

The error due to differences between the simulation- and the real temperature- (and humidity-) profile was evaluated by comparing the atmospheric transmittances derived from a real example radiosonde profile to transmittance using the standard profiles. This effect introduces an error to the pure absorption transmittance of around 2 % (depending on the band). To estimate the uncertainty due to the surface background information, the surface temperature was shifted by 5 K and the surface pressure was

AMTD
7, 7753–7792, 2014

perturbed by 20 hPa and subsequently committed to the transmittance forward operator. Again, $(\Delta L)^2$ is calculated and added to $\mathbf{S_e}$.

The spectral dependency of the surface reflectance is parametrized with the Normalized Differenced Vegetation Index (NDVI) (for further details see Lindstrot et al., 2012). The uncertainties of the surface reflectance range from 0.5 to 1.2 %. Similar to the approach pictured above, a perturbed TOA radiance is calculated and the resulting deviation is contributed to $\mathbf{S_e}$. Finally the residual model error, that is the difference between measurement and modeled radiance from the last iteration step is added to the measurement covariance matrix that consists of the sensor noise (see Table 1).

3.4 Validation datasets

The MODIS TCWV retrieval was validated against different ground-based measurements such as MicroWave Radiometer (MWR) data, GNSS water vapour monitoring data, and GCOS Upper Air Network (GUAN) radiosonde data.

3.4.1 ARM microwave radiometer

A data-set of ground-based MWR (software version 4.13) of three ARM (Atmospheric Radiation Measurement) sites (North Slope of Alaska (NSA), Southern Great Planes (SGP), Tropical Western Pacific (TWP)) for the years between 2002 and 2012 was used for the assessment of the TCWV retrieval. MWR instruments measure the radiation emitted by the atmospheric water vapour and liquid water at frequencies of 23.8 and 31.4 GHz (Turner et al., 2007). The background of the measurement is the cosmic background temperature. Consequently, it is one of the most accurate methods to determine the TCWV from ground. The uncertainty of the measured TCWV from MWR is expected to be in the range of 0.3 mm (Turner et al., 2003). This data-set was used to calculate the correction coefficients (see Sect. 4).

AMTD
7, 7753–7792, 2014

3.4.2 Ground-based GNSS

The global two-hourly GNSS TCWV data-set is based on three different resources: the International GNSS Service (IGS), U.S. SuomiNet (UCAR/COSMIC) products and Japanese GEONET data (Wang et al., 2007). Data from 942 stations for the years between 2003 and 2011 were extracted. The uncertainty of this data is not precisely stated by the author but a similar data-set provides an accuracy of 1–2 mm (Gendt et al., 2004).

3.4.3 GUAN radiosonde

A global data-set of TCWV derived from GUAN radiosondes, distributed via the Ground Tracking System (GTS) network and extracted from the DWD (Deutscher Wetterdienst) archive, was used to compare to the MODIS TCWV retrieval for the period 2003–2005. As radiosondes do not measure the whole vertical column at once, the accumulated TCWV has a relatively high uncertainty which can range between 1 and 10 % (Turner et al., 2003).

4 Correction

For reasons of clarity and comprehensibility, unless noted otherwise, only data of MODIS from the Aqua platform is used in the following. Nevertheless, the retrieval and the validation was also applied to Terra-data. In order to evaluate the performance of the retrieval, TCWV values were compared to ground-based Microwave radiometers (MWR) measurements. This data was considered as ground truth and compared to retrieved TCWV from collocated MODIS scenes. In order to assess the behavior of each band, a one-band-retrieval has been established that iteratively fits the simulated to the measured radiance for just one band using the same architecture and look-up tables as the three-band algorithm. The comparison of MODIS-derived TCWV against MWR data reveals different deviations in each band (see Fig. 4). On the one hand, the two

AMTD
7, 7753–7792, 2014

data-sets correlate linearly and the scattering is very low. On the other hand, there are significant differences, maximal (around 10 %) in case of the retrieval using just band 18 and minimal in case of the band 17 of around 3 %. When using band 18 or 19, the retrieval overestimates the TCWV, whereas band 17 has a small dry bias. These deviations add up to a wet-bias in the three-band retrieval of −0.6 mm (see Fig. 6). Reasons for this could be:

a. a systematic error of the MWR

b. a wrong spectral calibration of the MODIS bands

c. errors in the forward model.

First, the MWR data is very precise. Turner et al. (2003) quantified a measurement uncertainty of 0.3 mm and secondly a bias in the MWR data would introduce the same TCWV-shift to every band. Consequently, the MWR error can not explain the different signs.

MODIS has a built-in so-called Spectro-Radiometric-Calibration-Assembly (SRCA) that calibrates all bands on-orbit and keeps track of all radiometric changes and degradation of the optics (Xiong and Barnes, 2006). Xie et al. (2006) stated an uncertainty of the central wavelength of maximal 0.1 nm for band 17. Nevertheless, we tested the influence of a shifted central wavelength for all absorption bands as follows. A forward operator for the pure absorption was established which is additionally dependent on the central wavelength. The shape of the relative response functions (RSF) and all other modules of the TCWV retrieval remained unchanged. The scattering factor was assumed to be independent of the central wavelength. Afterwards, for each band TOA-radiances were simulated taking the TCWV values from the MWR validation database and compared to the measured values.

Figures 8 and 9 show the bias (upper row) and the bias corrected root mean square deviation (RMSD) (lower row) between simulated and measured radiances as a function of the considered central wavelength for each of the 10 detectors of the three

AMTD
7, 7753–7792, 2014

absorption bands. The dashed vertical lines indicates the nominal central wavelengths of the bands. The outcomes of this study are the following:

The sensitivities to the central wavelength (here the slope of the curves) differ between the bands as they are located in different parts of the spectrum with different absorption strengths. Additionally, the sensitivities increase with decreasing bandwidth, as expected. The zero of the bias (indicated by the vertical dotted lines) are shifted dissimilarly in different directions with different distance to the original nominal wavelength. These shifts would be necessary to cancel out all systematic differences between simulated and measured radiances. The shifts range from around 0.5 nm at Terra-band 18 to 4 nm at Terra-band 19. This exceeds by far the accuracy given by Xie et al. (2006). However, there are different shifts between MODIS Aqua (Fig. 8) and MODIS Terra (Fig. 9) (e.g. Aqua-band 19 and Terra-band 19). This implies that the specific sensor characteristics differ and that they could be a reason for the deviations between forward model and measurements although SRCA provides a high accuracy.

Furthermore, there are differences between individual detectors, especially in Aqua-band 18 and Terra-band 19. Here, one detector has a significant deviation to the others, respectively.

Another source of the differences between the simulated and measured radiances could be the forward operator of the retrieval. As presented in Sect. 2, the backbone of the forward operator is the determination of the atmospheric transmission due to water vapour absorption, T_{noscat}, and the the scattering factor f.

The latter is mainly dependent on the surface reflectance which is fairly constant for the validation data-set (0.2–0.3). At the same time, the aerosol properties such as AOD, scale height, aerosol type, can change a lot over the year. First of all, this would not introduce a systematic bias but rather an increased scattering. Secondly, the sensitivities of the AOD and scale height in respect to the simulated TCWV do not explain the deviations: Table 3 shows the influence of a doubled AOD, and Table 4 shows the influence of the aerosol scale height to the simulated TCWV for different surface reflectances. The error due to the different aerosol type is maximal around

AMTD
7, 7753–7792, 2014

0.5 % (not shown here). The sensitivities were calculated by deriving the difference of transmittance between an unperturbed and a perturbed AOD, and scale height respectively. The difference in transmittance has been transformed into an equivalent TCWV value using a partial derivative of transmittance with respect to TCWV. Supplementary, Diedrich et al. (2013) stated the low impact of the AOD on the error of a TCWV retrieval. However, the scattering-absorption interaction can be over- or underestimated in the radiative transfer simulations. The other potential source of error could be the determination of the absorption coefficients. Here, either the data-base of absorption coefficients, or the binning method could be wrong.

In summary, the origin of the deficiency of the retrieval is not exactly known yet. Hence, we introduce correction coefficients in order to adjust the atmospheric transmittance T_{noscat} in the optical thickness space. The corrected transmittance T_{corr} is then calculated by:

$$T_{\text{corr}} = \exp(a + b \cdot \ln(T_{\text{noscat}})). \quad (7)$$

The coefficients a and b were obtained beforehand by optimizing the difference between the simulated and measured atmospheric transmittance ($T_{\text{corr}} - T_{\text{meas}}$) using the MWR validation data-set as a reference (see Fig. 5). The uncorrected transmittance T_{noscat} was calculated by the absorption forward operator taking viewing geometries from MODIS and the TCWV information from the corresponding MWR measurement. T_{meas} was derived by:

$$T_{\text{meas}}(\lambda) = L_{\text{meas}}(\lambda)/L_0(\lambda) \quad (8)$$

where L_{meas} is the measured radiance in the absorption band. L_0 is the radiance presuming no absorption of water vapour. It is derived from interpolating the measured radiances (corrected for water vapour) in the window bands onto the position of the absorption band:

$$L_0(\lambda) = [(L_2/T_2 - L_5/T_5)/(\lambda_2 - \lambda_5)] \cdot (\lambda - \lambda_2) + L_2/T_2. \quad (9)$$

AMTD
7, 7753–7792, 2014

This was done separately for each band and for MODIS-Aqua and MODIS-Terra separately. The derived correction coefficients can be seen in Table 5 and 6. In the retrieval the transmittance is always corrected after Eq. (7). Figure 7 shows the flow of the correction- and validation process. As a consequence, the difference to ground-based measurements is reduced to a minimum, as can be seen in the next section.

5 Validation

The validation results are shown in Fig. 10. In each plot, the normalized relative frequency of occurrence is shown in grey shading with high occurrences plotted in bright grey to white, and low occurrences in black. In the top left corner of each plot the offset and slope of the linear regression, the bias corrected root mean square deviation (RMSD), the bias, the correlation coefficient, and the sample size as number of points (NPTS) are given.

Each data set was filtered for outliers and cloud contamination. The individual filter criteria are presented in the following subsections. MODIS measurements were spatially averaged over an area of 20 km × 20 km (20 pixel × 20 pixel) to account for e.g. the radiosonde displacement, the limited accuracy of the MODIS geolocation, and the time gap between satellite overpass and ground-based measurement. Additionally, all outliers (deviation $> 3\sigma$) were rejected. The location of all considered sites from the different data-sets are displayed in Fig. 2.

5.1 ARM MWR

As expected in Section. 4, the comparison of TCWV values of the corrected retrieval and the MWR show almost perfect agreement, although the number of samples is relatively low due to cloud contamination at the NSA and TWP sites. Thus, SGP provides 70 % of the number of points in the upper left panel of Fig. 10). Nevertheless, the data-set is representative for global observations because dry northern, wet tropical and mid

AMTD
7, 7753–7792, 2014

latitude conditions are contained. Only cases with 100 % valid MODIS pixels were considered to exclude the influences of clouds. The bias is 0.01 mm, the RMSD is 0.98 mm and the linear fit has a slope of 1 and an offset of −0.16.

5.2 Ground-based GNSS

We extracted GNSS-TCWV-data by taking all collocations with a time difference of one hour between measurement and satellite over-path. Here again, only cases with 100 % valid MODIS pixels were considered. The upper right panel of Fig. 10 shows the comparison between the GNSS- and MODIS- derived TCWV values. Although the filtering was very strict, the number of samples is still very high due to the high number of GNSS-stations. The bias is −0.8 mm, the RMSD is 1.9 mm indicating a slight overestimation of MODIS TCWV values. The linear fit has a slope of 0.98 and an offset of 1.12.

5.3 GUAN radiosonde

In order to account for the displacement of the radiosonde during its ascent, only cases with a time difference of maximum two hours between radiosonde and MODIS measurement were considered. In order to account for cloud contamination but also preserve a sufficient high number of data-points, only cases with less than 50 % valid MODIS pixel were rejected. The lower panel of Fig. 10 shows a bias of −1.6 mm and a RMSD of 3.1 mm. These values are in the range of the radiosonde uncertainty (Turner et al., 2003; Miloshevich et al., 2004). The linear fit has the slope of 0.97 and an offset of 2, although the correlation coefficient is relatively low (0.93).

5.4 Time dependency

In order to study the constancy of the accuracy of the retrieval the bias between the retrieved TCWV and GNSS / MWR was calculated as function of time (year) and plotted in Fig. 11. The annual difference between MWR and MODIS is close to zero for both

AMTD
7, 7753–7792, 2014

Aqua and Terra and constant over the years taking into account the large standard deviation. Whereas the bias between GNSS and and MODIS is shifted to negative values (meaning that MODIS values are generally higher than GNSS). There is also an apparent annual dependency with maximum at 2006 and minimum at the end of the time series. However, this oscillation is not significant considering the large standard deviation.

6 Summary and outlook

We present a retrieval of TCWV from MODIS measurements for cloud-free land-scenes in the near infrared spectral range. The 1-D-Var algorithm is based on a fast forward operator which basic functionality has been adapted from Lindstrot et al. (2012). Three main sub-procedures derive the surface reflectance, transmittance due to atmospheric water vapour and the shortening of the photon path due to atmospheric scattering respectively. A realistic uncertainty estimate is given on a pixel-by-pixel basis where measurement- and forward-model-uncertainties are considered.

An extensive validation study against several ground based reference data-sets reveals the high accuracy and precision of the retrieved TCWV values with bias corrected root mean square deviations between 1 mm (ARM MWR measurements), 2 mm (GNSS measurements) and 3.2 mm (GUAN radiosondes). The bias has been reduced to a minimum due to the introduction of correction coefficients for the transmittance calculation within the forward operator (0.1 mm to ARM MWR measurements, −0.8 mm to GNSS measurements, −1.6 mm to GUAN radiosondes). The scattering of the comparison between TCWV values from MODIS and ground based measurements is in the range of the retrieval uncertainty between 2 and 3 %.

It is intended to use transmission correction not only to increase the accuracy, but to homogenize time series of TCWV over land from different satellites and to use MODIS data as a gap filler between Medium Resolution Imaging spectrometer (MERIS) and the Ocean and Land Color Instrument (OLCI). Due to the fact that the data-sets overlap,

AMTD
7, 7753–7792, 2014

MERIS and OLCI could be emulated with MODIS in order to inter-compare the TCWV time series.

Acknowledgements. This work was partly performed in the frame of the WadaMo project (DLR – BMWi) and HD(CP)^2 (BMBF). The authors would like to thank Marc Schröder from DWD for providing the GNSS data.

References

Albert, P., Bennartz, R., and Fischer, J.: Remote sensing of atmospheric water vapor from backscattered sunlight in cloudy atmospheres, J. Atmos. Ocean. Tech., 18, 865–874, doi:10.1175/1520-0426(2001)018<0865:RSOAWV>2.0.CO;2, 2001. 7758

Albert, P., Bennartz, R., Preusker, R., Leinweber, R., and Fischer, J.: Remote sensing of atmospheric water vapor using the moderate resolution imaging spectroradiometer, J. Atmos. Ocean. Tech., 22, 309, doi:10.1175/JTECH1708.1, 2005. 7758

Bartsch, B., Bakan, S., and Fischer, J.: Passive remote sensing of the atmospheric water vapour content above land surfaces, Adv. Space Res., 18, 25–28, doi:10.1016/0273-1177(95)00285-5, 1996. 7758

Diedrich, H., Preusker, R., Lindstrot, R., and Fischer, J.: Quantification of uncertainties of water vapour column retrievals using future instruments, Atmos. Meas. Tech., 6, 359–370, doi:10.5194/amt-6-359-2013, 2013. 7768

Fell, F. and Fischer, J.: Numerical simulation of the light field in the atmosphere-ocean system using the matrix-operator method, J. Quant. Spectrosc. Ra., 69, 351–388, doi:10.1016/S0022-4073(00)00089-3, 2001. 7761

Fischer, J. and Grassl, H.: Radiative transfer in an atmosphere-ocean system: an azimuthally dependent matrix-operator approach, Appl. Optics, 23, 1032–1039, doi:10.1364/AO.23.001032, 1984. 7761

Fraser, R. S., Ferrare, R. A., Kaufman, Y. J., Markham, B. L., and Mattoo, S.: Algorithm for atmospheric corrections of aircraft and satellite imagery, Int. J. Remote Sens., 13, 541–557, doi:10.1080/01431169208904056, 1992. 7758

AMTD
7, 7753–7792, 2014

Gao, B.-C. and Kaufman, Y. J.: Water vapor retrievals using Moderate Resolution Imaging Spectroradiometer (MODIS) near-infrared channels, J. Geophys. Res.-Atmos., 108, 4389, doi:10.1117/12.154909, 2003. 7755, 7756, 7761

Gao, B.-C., Goetz, A. F. H., Westwater, E. R., Conel, J. E., and Green, R. O.: Possible near-IR channels for remote sensing precipitable water vapor from geostationary satellite platforms., J. Appl. Meteorol., 32, 1791–1801, doi:10.1175/1520-0450(1993)032<1791:PNICFR>2.0.CO;2, 1993. 7758

GCOS: World Meteorological Organization: Guideline for the Generation of Datasets and Products Meeting GCOS Requirements (GCOS-143), https://www.wmo.int/pages/prog/gcos/Publications/gcos-143.pdf (last access: 28 July 2014), 2010. 7755

Gendt, G., Dick, G., Reigber, C., Tomassini, M., Liu, Y., and Ramatschi, M.: Near real time GPS water vapor monitoring for numerical weather prediction in Germany, J. Meteorol. Soc. Jpn., 82, 361–370, 2004. 7765

Hansen, J. E. and Travis, L. D.: Light scattering in planetary atmospheres, Space Sci. Rev., 16, 527–610, doi:10.1007/BF00168069, 1974. 7758

Hollstein, A. and Fischer, J.: Radiative transfer solutions for coupled atmosphere ocean systems using the matrix operator technique, J. Quant. Spectrosc. Ra., 113, 536–548, doi:10.1016/j.jqsrt.2012.01.010, 2012. 7761

Lindstrot, R. and Preusker, R.: On the efficient treatment of temperature profiles for the estimation of atmospheric transmittance under scattering conditions, Atmos. Meas. Tech., 5, 2525–2535, doi:10.5194/amt-5-2525-2012, 2012. 7759

Lindstrot, R., Preusker, R., Diedrich, H., Doppler, L., Bennartz, R., and Fischer, J.: 1D-Var retrieval of daytime total columnar water vapour from MERIS measurements, Atmos. Meas. Tech., 5, 631–646, doi:10.5194/amt-5-631-2012, 2012. 7755, 7756, 7759, 7760, 7764, 7771

Lindstrot, R., Stengel, M., Schröder, M., Fischer, J., Preusker, R., Schneider, N., and Steenbergen, T.: A global climatology of total columnar water vapour from SSM/I and MERIS, Earth Syst. Sci. Data Discuss., 7, 59–88, doi:10.5194/essdd-7-59-2014, 2014. 7755

McClatchey, R., Fenn, R., Selby, J., Volz, F., and Garing, J.: Optical Properties of the Atmosphere, 3rd Edn., Tech. Rep., Air Force Cambridge Research Laboratories, 1972. 7761

Miloshevich, L. M., Paukkunen, A., Vömel, H., and Oltmans, S. J.: Development and validation of a time-lag correction for Vaisala radiosonde humidity measurements, J. Atmos. Ocean. Tech., 21, 1305, doi:10.1175/1520-0426(2004)021<1305:DAVOAT>2.0.CO;2, 2004. 7770

AMTD
7, 7753–7792, 2014

Noël, S., Buchwitz, M., Bovensmann, H., and Burrows, J. P.: Retrieval of total water vapour column amounts from GOME/ERS-2 data, Adv. Space Res., 29, 1697–1702, doi:10.1016/S0273-1177(02)00099-6, 2002. 7755

Pougatchev, N., August, T., Calbet, X., Hultberg, T., Oduleye, O., Schlüssel, P., Stiller, B., Germain, K. St., and Bingham, G.: IASI temperature and water vapor retrievals – error assessment and validation, Atmos. Chem. Phys., 9, 6453–6458, doi:10.5194/acp-9-6453-2009, 2009. 7755

Rodgers, C.: Inverse Methods for Atmospheric Sounding: Theory and Practice, World Scientific Pub Co., 2000. 7762, 7763

Rothman, L. S., Rinsland, C. P., Goldman, A., Massie, S. T., Edwards, D. P., Flaud, J.-M., Perrin, A., Camy-Peyret, C., Dana, V., Mandin, J.-Y., Schroeder, J., McCann, A., Gamache, R. R., Wattson, R. B., Yoshino, K., Chance, K., Jucks, K., Brown, L. R., Nemtchinov, V., and Varanasi, P.: Reprint of: The HITRAN molecular spectroscopic database and HAWKS (HITRAN Atmospheric Workstation): 1996 edition, J. Quant. Spectrosc. Ra., 111, 1568–1613, doi:10.1016/j.jqsrt.2010.04.019, 2010. 7784

Schluessel, P. and Emery, W. J.: Atmospheric water vapour over oceans from SSM/I measurements, Int. J. Remote Sens., 11, 753–766, doi:10.1080/01431169008955055, 1990. 7755

Trenberth, K. E., Fasullo, J., and Smith, L.: Trends and variability in column-integrated atmospheric water vapor, Clim. Dynam., 24, 741–758, doi:10.1007/s00382-005-0017-4, 2005. 7755

Turner, D. D., Lesht, B. M., Clough, S. A., Liljegren, J. C., Revercomb, H. E., and Tobin, D. C.: Dry bias and variability in Vaisala RS80-H radiosondes: The ARM experience, J. Atmos. Ocean. Tech., 20, 117–132, doi:10.1175/1520-0426(2003)020<0117:DBAVIV>2.0.CO;2, 2003. 7764, 7765, 7766, 7770

Turner, D. D., Clough, S. A., Liljegren, J. C., Clothiaux, E. E., Cady-Pereira, K. E., and Gaustad, K. L.: Retrieving liquid water path and precipitable water vapor from the atmospheric radiation measurement (ARM) microwave radiometers, IEEE T. Geosci. Remote, 45, 3680–3690, doi:10.1109/TGRS.2007.903703, 2007. 7764

Wang, J., Zhang, L., Dai, A., van Hove, T., and van Baelen, J.: A near-global, 2-hourly data set of atmospheric precipitable water from ground-based GPS measurements, J. Geophys. Res.-Atmos., 112, D11107, doi:10.1029/2006JD007529, 2007. 7765

Xie, Y., Xiong, X., Qu, J. J., and Che, N.: Uncertainty analysis of Terra MODIS on-orbit spectral characterization, in: Society of Photo-Optical Instrumentation Engineers (SPIE) Conference

AMTD
7, 7753–7792, 2014

Series, vol. 6296 of Society of Photo-Optical Instrumentation Engineers (SPIE) Conference Series, doi:10.1117/12.680766, 2006. 7766, 7767
Xiong, X. X. and Barnes, W.: An overview of MODIS radiometric calibration and characterization, Adv. Atmos. Sci., 23, 69–79, doi:10.1007/s00376-006-0008-3, 2006. 7766, 7776

AMTD
7, 7753–7792, 2014

Table 1. Position and widths of five NIR bands (original MODIS design specification) used for the TCWV retrieval (Xiong and Barnes, 2006).

MODIS band	position [nm]	width [nm]	SNR
2	865	40	201
5	1240	20	74
17	905	30	167
18	936	10	57
19	940	50	250

AMTD
7, 7753–7792, 2014

Table 2. Regression coefficients between transmittance and TCWV for the determination of the first guess from the transmittance of band 17.

	c3	c2	c3
coefficients	0.0746699	−1.15649	19.9892

AMTD
7, 7753–7792, 2014

Table 3. Influence of a doubled AOD to the simulated TCWV for different surface reflectances in units of TCWV (mm) for a retrieval using only one absorption band.

surface reflectance	band 17	band 18	band 19
0.1	−0.110	−0.344	−0.255
0.3	0.153	0.018	0.076
0.9	0.442	0.328	0.376

AMTD
7, 7753–7792, 2014

Table 4. Influence of the aerosol scale height to the simulated TCWV for different surface reflectances in units of TCWV (mm) for a retrieval using only one absorption band.

surface reflectance	band 17	band 18	band 19
0.1	−0.463	−1.035	−0.793
0.3	−0.017	−0.288	−0.172
0.9	0.279	0.074	0.153

AMTD
7, 7753–7792, 2014

Table 5. Correction coefficients for the adjustment of the transmittance due to water vapour for each band on MODIS Aqua.

coefficients	band 17	band 18	band 19
a	0.016349	0.028888	0.030634
b	0.996429	1.033570	1.048570

AMTD
7, 7753–7792, 2014

Table 6. Correction coefficients for the adjustment of the transmittance due to water vapour for each band on MODIS Terra.

coefficients	band 17	band 18	band 19
a	0.027142	0.035238	0.032857
b	1.010710	1.065710	1.063210

AMTD
7, 7753–7792, 2014

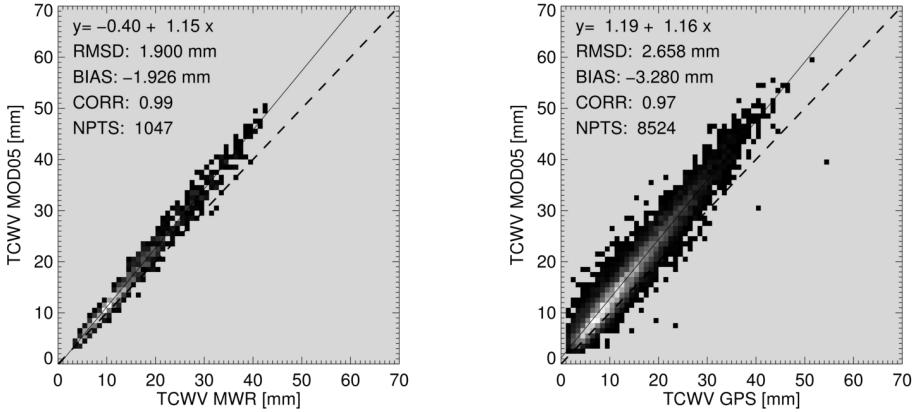

Figure 1. Normalized frequencies of occurrence for the comparison of the MODIS L2-TCWV-product (MOD05) against ground-based microwave radiometers (3 sites: ARM SGP, TWP, NSA; left panel) and global ground-based GNSS-data (right panel), each for the period 2003–2011. Figure 2 shows the geographical distribution of the validation data. See text for detailed information.

AMTD
7, 7753–7792, 2014

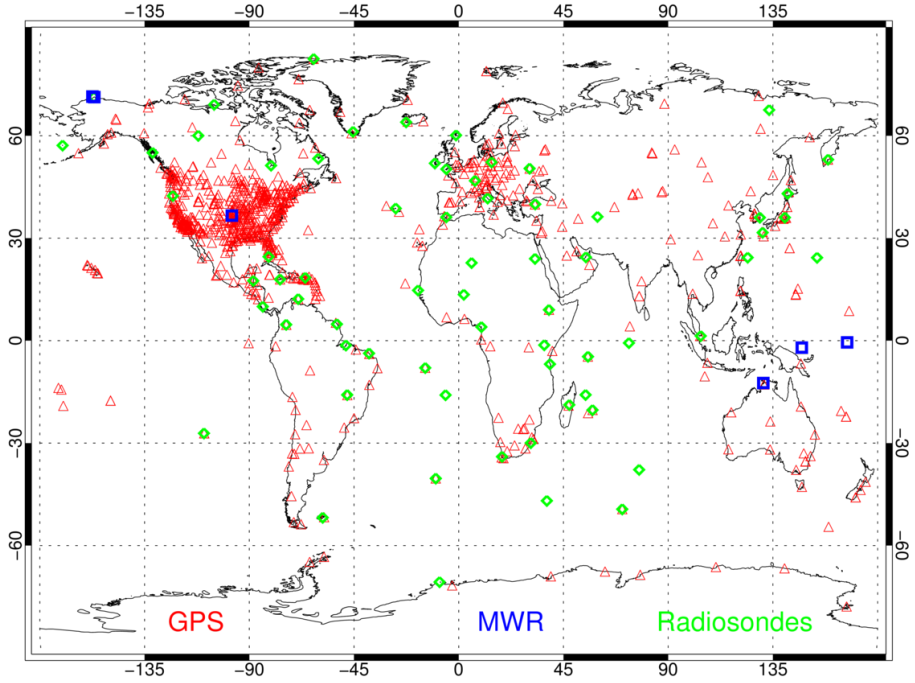

Figure 2. Geographic distribution of used validation data over land (MWR: Microwave radiometer stations, GPS: GNSS stations, Radiosonde: GUAN radiosonde stations).

AMTD
7, 7753–7792, 2014

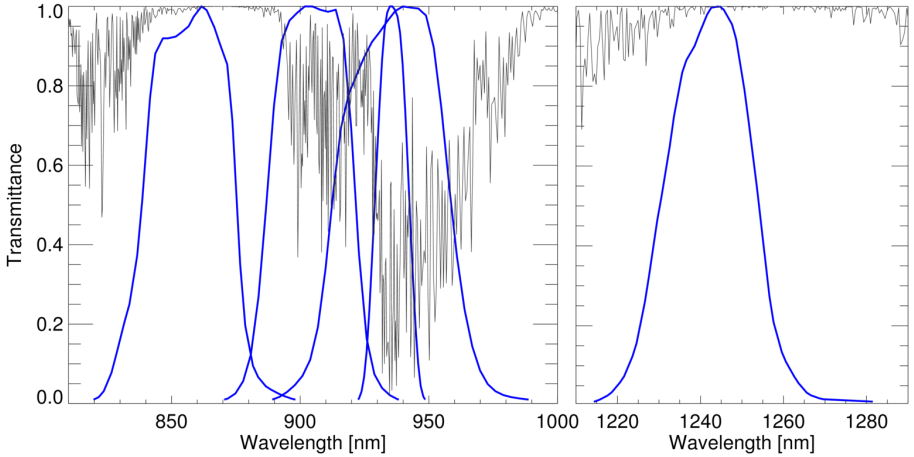

Figure 3. Simulated total atmospheric Transmittance due to water vapour in the NIR (absorption coefficients from HITRAN-database, Rothman et al., 2010; black curve) and actual relative response function of the five used MODIS Aqua bands (blue curves).

AMTD
7, 7753–7792, 2014

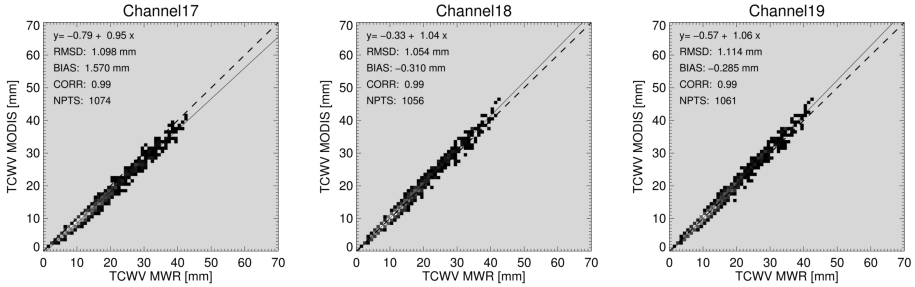

Figure 4. Normalized frequencies of occurrence for comparisons of TCWV retrieved from the MODIS-retrieval just using one absorption band against MWR TCWV data; see text for detailed description.

AMTD
7, 7753–7792, 2014

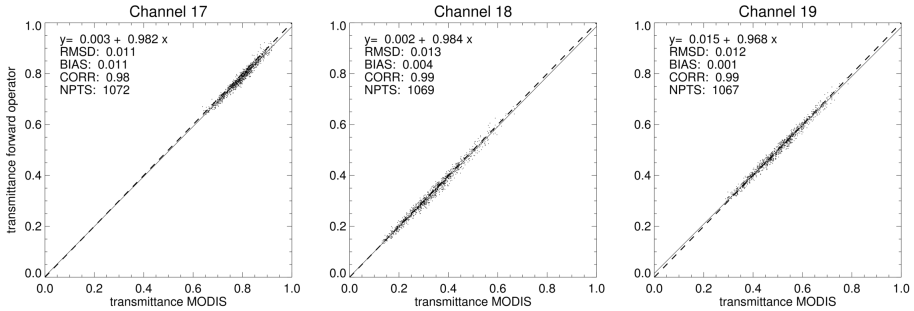

Figure 5. Simulated versus measured atmospheric transmittances due to water vapour for each MODIS band using the same data as in Fig. 4; see Sect. 4 for detailed description of the compared variables.

AMTD
7, 7753–7792, 2014

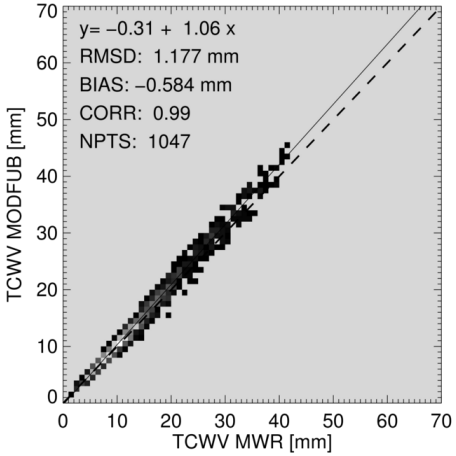

Figure 6. Normalized frequencies of occurrence for comparisons of the TCWV retrieved from the uncorrected MODIS-retrieval against MWR TCWV data; see text for detailed description.

AMTD
7, 7753–7792, 2014

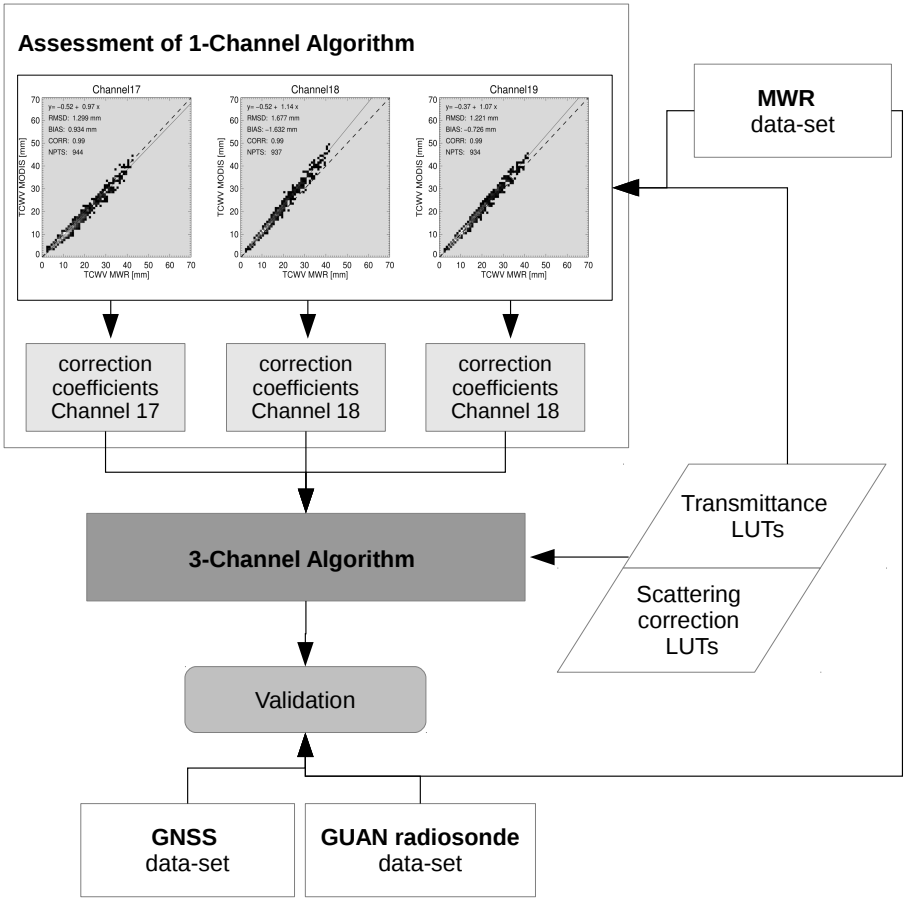

Figure 7. Flowchart of the correction and validation process.

AMTD
7, 7753–7792, 2014

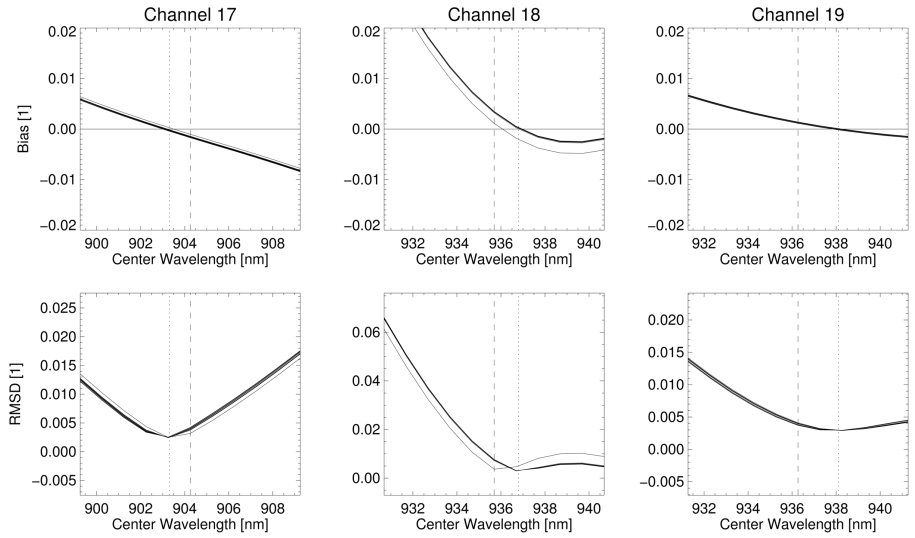

Figure 8. Assessment of the radiance – central wavelength dependency for MODIS-Aqua: Bias (upper row) and RMSD (lower row) between simulated and measured radiances as a function of the assumed central wavelength for each absorption band. Each curve represents one of the 10 detectors. The vertical dashed lines indicate the position of the original nominal wavelength of the band. The vertical doted lines indicate the position of zero bias and minimum RMSD. See text for further discussion (Sect. 4).

AMTD
7, 7753–7792, 2014

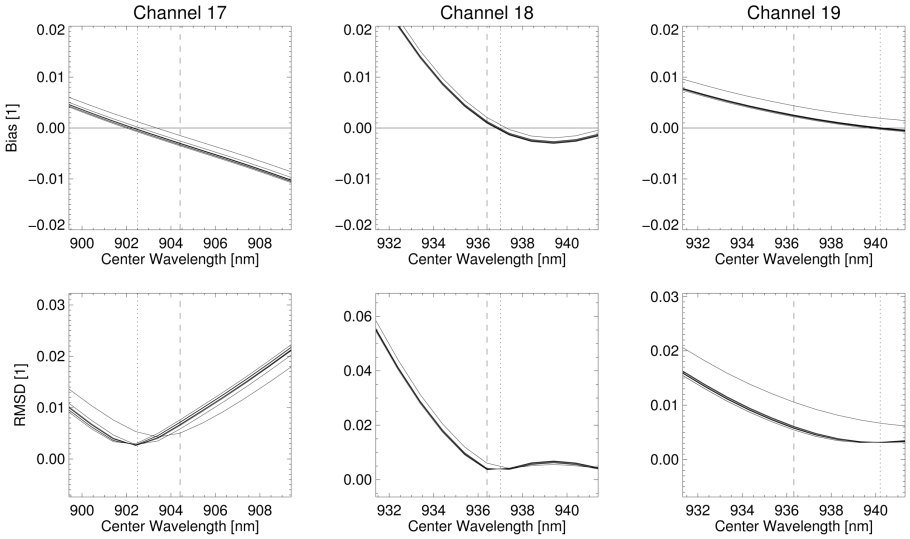

Figure 9. Assessment of the radiance – central wavelength dependency for MODIS-Terra: Bias (upper row) and RMSD (lower row) between simulated and measured radiances as a function of the assumed central wavelength for each absorption band. Each curve represents one of the 10 detectors. The vertical dashed lines indicate the position of the original nominal wavelength of the band. The vertical doted lines indicate the position of zero bias and minimum RMSD. See text for further discussion (Sect. 4).

AMTD
7, 7753–7792, 2014

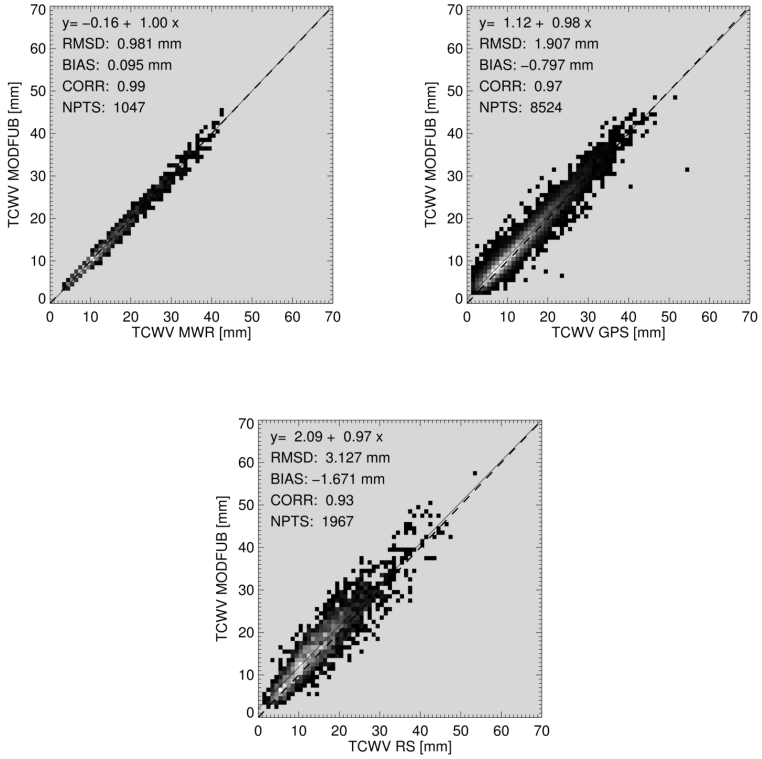

Figure 10. Normalized frequencies of occurrence for the comparison of the TCWV-retrieval against ground-based microwave radiometers (upper left panel) and global ground-based GNSS-data (upper right panel), and GUAN Radiosonde data (lower Panel). For detailed description see Sects. 3.4 and 5.

AMTD
7, 7753–7792, 2014

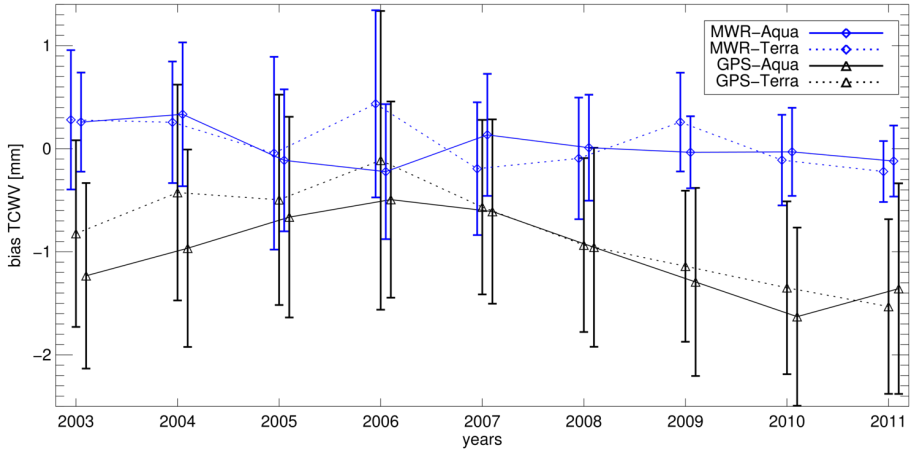

Figure 11. Annual bias in mm between TCWV retrieved from MODIS Aqua (doted lines: MODIS-Terra) and ground-based measurements (blue: MWR, black: GNSS); vertical bars indicate the standard deviation for each year.

AMTD
7, 7753–7792, 2014